HHS Public Access

Author manuscript

Macromolecules. Author manuscript; available in PMC 2025 June 30.

Published in final edited form as:

Macromolecules. 2024 December 24; 57(24): 11688–11696. doi:10.1021/acs.macromol.4c01874.

Lipid Membrane Leaflets Unzip upon Hybridization with Polymer-Rich Nanodomains

James F. Tallman[‡],
Department of Materials Science and Engineering, Grainger College of Engineering, University of Illinois at Urbana—Champaign, Urbana, Illinois 61801, United States

Nurila Kambar[‡],
Department of Materials Science and Engineering, Grainger College of Engineering, University of Illinois at Urbana—Champaign, Urbana, Illinois 61801, United States

Cecília Leal,
Department of Materials Science and Engineering, Grainger College of Engineering, University of Illinois at Urbana—Champaign, Urbana, Illinois 61801, United States

Antonia Statt
Department of Materials Science and Engineering, Grainger College of Engineering, University of Illinois at Urbana—Champaign, Urbana, Illinois 61801, United States

Abstract

There is a long-term interest in creating artificial biomimetic membranes where self-assembled phospholipid bilayers are selectively permeabilized by synthetic channel-like molecules. One example is the coassembly of amphiphilic block copolymers with phospholipids into a hybrid membrane. Hybrid phospholipid block copolymer bilayers display many properties, seen in biomembranes such as selective transport phenomena, synergistic elastic properties, and structural phase transformations. Just like in biomembranes, these fundamental properties of hybrid bilayers are often regulated by lateral phase separation. Understanding the molecular and physical cues that determine the formation of rafts or domains in hybrid membranes, their size, and morphology is paramount to elucidating and programming their function. Employing a combination of coarse-grained molecular dynamics simulations and high-resolution cryogenic electron microscopy, we discovered that phosphatidylcholine-cholesterol bilayers hybridized with poly(butadiene-*b*-ethylene oxide) develop two distinct phase-separated morphologies. At molar fractions of polymer above 10 mol % the expected molecular distribution into lipid-rich and polymer-rich domains is

Corresponding Authors: Cecília Leal – *Department of Materials Science and Engineering, Grainger College of Engineering, University of Illinois at Urbana—Champaign, Urbana, Illinois 61801, United States;* cecilial@illinois.edu, **Antonia Statt** – *Department of Materials Science and Engineering, Grainger College of Engineering, University of Illinois at Urbana—Champaign, Urbana, Illinois 61801, United States;* statt@illinois.edu.

‡Author Contributions

‡J.F.T. and N.K. contributed equally to this work.

The authors declare no competing financial interest.

Complete contact information is available at: https://pubs.acs.org/10.1021/acs.macromol.4c01874

ASSOCIATED CONTENT

Supporting Information

The Supporting Information is available free of charge at https://pubs.acs.org/doi/10.1021/acs.macromol.4c01874.

Simulation model validation, additional simulation of hybrid membranes, and additional cryo-EM images (PDF)

observed. However, at low polymer content, a new structure develops in which the bilayer leaflets unzip (but remain continuous) to incorporate nanodomains of hydrophobic butadiene globules. We conjecture that unzipping is energetically more favorable than sustaining the hydrophobic mismatch between butadiene blocks and phospholipid acyl chains. These findings offer new insights into the morphology of biomembranes upon the insertion of transmembrane proteins with bulky hydrophobic residues.

Graphical Abstract

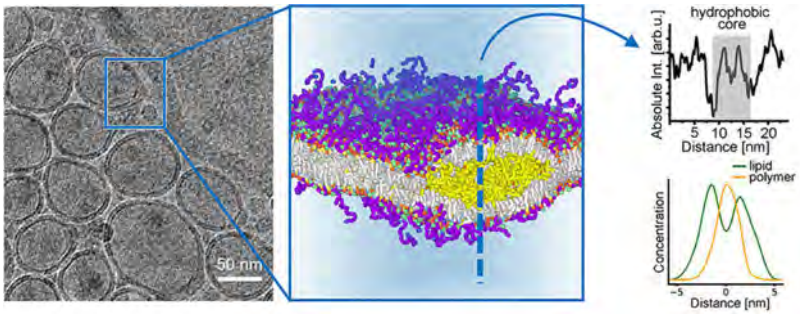

INTRODUCTION

Effective materials and methods for creating biomimetic cell membranes[1,2] are essential for understanding biological processes of selective transport and for the development of new systems relevant for biotechnology and pharmaceuticals.[3,4] The most fundamental artificial membrane was developed 25 years ago by Hammer and co-workers[5] where, akin to biological phospholipids, amphiphilic block copolymers self-assemble into bilayer vesicles having radii ranging from 50 nm to 5 μm or more. Polymer- and lipid-based membranes can adopt analogous yet diverse forms[6,7] but have distinct mechanical properties, permeability, and lateral diffusivity. Amphiphilic block copolymers have enormous chemical versatility by incorporating functional groups with selectivity to small molecules, ions, and charges. This has motivated the effort to create chimeric membranes, engineered to integrate the desired properties from both lipid and polymeric components.[8–16] Such hybrid membranes have been shown to be advantageous in a number of applications such as hydrophobic drug encapsulation and directed drug permeation,[9–11,13] protein folding/activity,[17–20] molecular[21,22] and heat transport,[23] as well as expanding the structural phase space.[14]

Similar to how biomembranes that are loaded with transmembrane proteins and cholesterol can form rafts,[24] insertion of amphiphilic polymers often results in the formation of polymer-rich and lipid-rich domains.[8,25–27] The enhanced properties of hybrid membranes are almost always controlled by the process of lateral phase separation and the in-membrane interactions between polymers and lipids. For example, we have shown that amorphous butadiene blocks, upon membrane insertion, can fluidize all-trans phospholipid acyl chains.[9,10] Moreover, highly hydrophobic drugs have been shown to accumulate at the interface between polymer and lipid domains,[11] leading to enhanced drug permeation.[9]

Understanding the process of domain formation in hybrid membranes, as well as characterizing the spatial distribution and in-membrane interaction of polymers and lipids with molecular detail, is fundamental to enabling the design and functionality of artificial membranes. This insight is essential to understand analogous membrane-based phenomena in biology, such as neutral fat accumulation in the endoplasmic reticulum bilayer at the onset of lipid droplet organelle biogenesis.[28] Moreover, nitrogen accumulation,[29] nanoplastics,[30] and nanoparticles[31,32] in lipid bilayers involve domain formation, as well as the synthesis of hydrophobic polymers in vesicles.[33–35] Insights into domain and macrophase separation in hybrid membranes will also help explain why these systems effectively suppress drug crystallization and enhance hydrophobic drug permeation.[9,10] Hybrid systems, in both bulk and nanoparticle forms, consistently outperform pure systems in encapsulating low-solubility drugs,[13] making them particularly advantageous for biotechnological and pharmaceutical applications.

Several studies of hybrid polymer–lipid membranes suggest that there are conditions at which microscale lipid-rich or polymer-rich domains[8,9,11,16,22,23,25,27,36–41] develop (which we refer to as type 1). Otherwise, lipids and polymers are said to molecularly mix.[8,21,42–47]

A myriad of tools[15] are available and have been used to inspect microscale domains such as optical microscopy, atomic force microscopy, and X-ray scattering,[8–11,13,14,25,26,38] normally characterizing two distinct membrane thicknesses.[9,10,13,25,37–39,48–50] However, nanodomains can be hard to distinguish from molecularly mixed systems.[8,21,42,43,45,46,51] With high-resolution cryogenic electron microscopy (cryo-EM), Beales and co-workers[52] identified populations of hybrid (POPC:PBD-*b*-PEO) nanoparticles with two distinct thickness; however, they never identified nm size domains. For a system with significant polymer content (≥20 mol %) we clearly observe coexisting thick polymer-rich and thin lipid-rich type 1 domains in hybrid vesicles (Figure 1d, left). Mesoscale simulations using dissipative particle dynamics have demonstrated the formation of type 1 nanodomains at high polymer concentrations with short polymer chains,[53] and coarse-grained molecular dynamics by Jeuken and co-workers[54] using the Martini model have suggested the coexistence of thick and thin phases.

While microscale domains are easy to detect and rationalize, the formation of several lateral nanodomains (which would generate many high-energy interfaces) is difficult to realize, especially for systems where there is a large hydrophobic mismatch (~5 nm) between polymers and lipids.[19,30,50,52,55,56] Solid-state nuclear magnetic resonance (ssNMR) data[10] suggest that, at the nanoscale, amorphous polymer blocks continuously fluidize lipid acyl chains. Otherwise, the available tools to characterize the structure of domains with molecular-level detail are rather limited, highlighting the need for computer simulation methods. In this work, we employ coarse-grained molecular dynamics simulations and high-resolution cryo-EM imaging to uncover a new phase separation morphology, type 2, in polymer–lipid hybrid membranes. We found conditions at which bilayer leaflets unzip to accommodate nanosized globules of self-assembled hydrophobic polymer blocks, demonstrating an intermediate phase separation behavior seen with inorganic and polymeric nanoparticles[31–35] but not self-assembled amphiphilic copolymers.

RESULTS AND DISCUSSION

We combine MD simulations with cryo-EM to investigate the composition regimes leading to different types of domains in membrane vesicles. Simulations were parametrized using Martini v3[57] and executed in isobaric–isothermal conditions (P_z = 1 atm, $P_x = P_y$ = 0 atm, T = 298 K) with HOOMD-blue.[58] Vesicles are prepared by microfluidic nanoprecipitation which is known to yield size and compositional uniformity.[13,59–62] The "lipid" inlet comprises ethanol-dissolved DPPC:Chol at a 50:50 mol % (1,2-dipalmitoyl-*sn*-*glycero*-3-phosphocholine:cholesterol) and polymer PBD-*b*-PEO (poly(butadiene-*b*-ethylene oxide) with PBD block of 2500 g/mol and PEO block of 1500 g/mol (PBD block rich in trans 1,4 microstructure), and the aqueous inlet is DI water (Figure 1a). While many studies use a shorter polymer,[52,54,55] we have chosen a relatively long polymer (46 monomer repeat units) to explore the hydrophobic mismatch between molecules of significantly different size, which form hybrid membranes as shown here. In addition, other studies used PBD rich in cis 1,2 microstructure.[52,54,55] We note that the two isomers possess similar Kuhn lengths and hydrophobicities, yielding similar macromolecular behavior.

Cryo-EM enables direct imaging of nanoscopic domains in biomembranes[63,64] and hybrid polymer–lipid membranes,[52] detecting (sub)nm variations in bilayer thickness. Figure 1d, left, shows a cryo-EM image of type 1 phase-separated hybrid (20 mol % block copolymer) vesicles, and Figure 1d, right, shows three samples at different compositions that were synthesized separately but mixed in the grid such that all vesicles are exposed to the same electron beam dosage. Three distinct membranes are clearly observed in Figure 1d, right: lipid-rich, thin, and darker due to phosphate groups (L), thicker, lower-density polymer-rich (P), and hybrid (10 mol % block copolymer) (H). Additional images of L, P (Figure S13, which shows assembly of both worm-like micelles and vesicles), and H vesicles are shown in Figures S10–S12. Figure 1b shows a simulation snapshot of a hybrid system comprising 10 mol % block copolymer. This indicates the presence of type 2 domains where lipid monolayers unzip to accommodate the PBD block, akin to a mixed lipid-block copolymer micelle (Figure 1c) embedded in the lipid bilayer. The cryo-EM image in Figure 1e is fully consistent with the MD result showing a lens-shaped domain in the membrane. A profile of the electron density of the lens domain (Figure 1g) shows a high-intensity peak due to the continuous presence of phosphate lipid headgroups at the domain interface. A zoomed-in image, electron density profile, and simulations (parts f, h, and c of Figure 1, respectively) clearly show that the lens domain has mixed-micelle character. The electron density profile analysis (Figure 1g,h) reveals distinct high-density regions corresponding to phospholipid headgroups and low-density regions representing hydrophobic bilayer cores, indicating the presence of PBD and lipid acyl chains within the lens-shaped nanodomain. These variations are evident in cryo-EM images, allowing us to differentiate between polymer (P), lipid (L), and hybrid (H) membranes.

While both type 1 and type 2 domains are polymer-rich with some amount of lipids, type 2 domains are distinct from the previously reported morphologies because of the presence of three qualities: (1) They contain a continuous monolayer of lipids on both sides of the leaflet (as shown in Figure 1b,e,g). (2) They exhibit the coexistence of thick and thin phases in a single nanoparticle. (3) The lipid and polymer phase-separate such that the polybutadiene

occupies the interior space of the bilayer. Type 1 domains satisfy only (2).[16] The thick but homogeneous membranes discussed by Beales and co-workers[52] satisfy (3) and potentially (1) but not (2). The realization of the type 2 domains suggests that these self-assembled systems have several mechanisms to resolve the hydrophobic mismatch inherent to a hybrid system. Likewise, we hypothesize that interfaces between type 1 domains in macrophase systems could contain similar "unzipped" regions near the interface to provide a gradual transition over the thickness mismatch.

Leaflet unzipping and the formation of membrane-embedded "fat" lenses are well-known in biomembranes during the process of lipid droplet (LD) biogenesis.[28] In-membrane liquid–liquid phase separation leads to neutral fat accumulation in lens-shape micelles at the midplane of the endoplasmic reticulum bilayer before LD budding. Analogous morphologies have been suggested, although not yet demonstrated experimentally, in processes such as microplastic aggregation[30] and nitrogen accumulation[29] within lipid membranes. The unzipping of lipid bilayers observed in our study is identical to phenomena seen in nanoparticle encapsulation within lipid membranes[31,32] and polymerization within membrane vesicles,[33–35] described as a "parachute" morphology. This is interesting because it shows that membranes indeed have a remarkable ability to deform out-of-plane to accommodate thick yet small cross-sectional-area polymer domains. However, an in-depth image analysis of the cryo-EM data would be needed to verify that bilayers do indeed remain continuous around the polymer globule in the "parachute" system.[33] In this paper, we clearly show by simulation and electron density analysis of cryo-EM data that bilayers unzip and enable type 2 domain formation, which is surprising because the polymer component is amphiphilic. This is a new finding, as until now the community working on amphiphilic polymer–lipid hybrid membranes has treated the integration of amphiphilic polymers into phospholipid bilayers as type 1 phase-separation into interfacing polymer-rich and lipid-rich domains that would only vary in size (from nm to μm), not morphology.

In the context of hybrid membranes, hydrophobic mismatch between PBD and lipid tails has been extensively discussed as the driving force for phase separation.[9,19,40,65] This hydrophobic mismatch comes from the longer PBD hydrophobic chains compared with the fully saturated DPPC. DOPC chains are even thinner than DPPC due to the presence of double bonds. Type 2 domains allow the PBD blocks and lipid tails to maximize self-interactions, minimizing the free energy of the system. Furthermore, type 2 domains are consistent with the two membrane thicknesses experimentally detected by cryo-EM and X-ray scattering. Unzipped bilayers act as a "surfactant" monolayer, explaining the significant increase in lipid fluidity with PBD-*b*-PEO hybridization shown by ssNMR.[10] When block copolymer content is increased to 20 mol %, type 1 phase separation is stable (Figure 1d, left). The domain sizes for type 1 and type 2 regions were determined to be approximately 65 and 23 nm, respectively, within a population of similarly sized vesicles. Although the domains appear relatively uniform in the cryo-EM images, it is important to recognize that while cryo-EM provides high-resolution structural information, it is not well-suited for reliably quantifying domain size distributions due to the inherently small sampling size.

Varying the polymer concentration is expected to influence the morphology and size of phase-separated domains in the DPPC:Chol:PBD-*b*-PEO membranes. Figure 2a displays simulation snapshots showing the evolution of domain morphology as polymer to lipid content is reduced. Concentration profiles across the membrane (Figure 2b) show symmetric leaflets, some cholesterol solubility in the polymer phase, and a clear preference for PBD toward the interior of membranes. The thickness (Figure 2c) and concentration maps (Figure 2d) show two types of phase separation. At low polymer concentration, lipid monolayers are continuous (type 2). At higher concentrations, the lipids begin to form rafts and recreate thick, polymer-like hybrid membranes.[40,52–55] The raft formation is evidenced by the local depletion of lipids in the concentration maps shown in Figure 2d. This behavior implies that above 20 mol % of polymer, the vesicle stability and mechanical properties are determined by the properties of the polymer. Likewise, the lipid rafts have elevated mobility, enabling the formation of larger type 1 domains. Additional simulations were performed for DPPC:PBD-*b*-PEO and DOPC (1,2-dioleoyl-*sn*-glycero-3-phosphocholine):PBD-*b*-PEO. In Figures S7 and S8 representative snapshots, thickness maps, and concentration maps are shown. Regardless of the lipid type, the morphologies match those discussed here for the DPPC:Chol:PBD-*b*-PEO system.

Figure 3a–d (and Figures S10 and S11) shows cryo-EM images of membrane vesicles comprising 0, 10, 20, and 100 mol % PBD-*b*-PEO. Pure lipid vesicles have thinner and more electron-dense membranes (due to phospholipid headgroups) than pure polymer vesicles (Figure 3a,d). At 20 mol % polymer, there is clear type 1 phase separation into lipid-rich and polymer-rich domains (Figure 3c, Figure 1d, left). At lower polymer content (≤10 mol %), a type 2 phase-separated lens-like domain is observable (Figure 3b, Figure 1d, right). Figure 3i–l displays corroborating simulation snapshot data for corresponding experimental compositions. These snapshots do not introduce different systems but complement and reinforce the experimental findings, providing a clearer connection between the simulations and the experimental data. The electron density profile analysis of the membrane regions (Figure 3e–-h) highlights electron-lucent hydrophobic bilayer cores, corresponding to the hydrocarbon chains of lipids or polymers, along with high-intensity phosphate regions within the lipid headgroups. This profile analysis is essential for confirming the structural integrity and continuity of the lipid bilayers, proviing direct experimental evidence of different types of phase separation in hybrid membranes. The electron density profiles allow us to visualize the integration of amphiphilic block copolymers with lipid bilayers, highlighting how the hydrophobic and hydrophilic components interact within the membrane. This analysis also reinforces the unzipped type 1 domain formation discussed in the study, offering a more detailed view of the possible membrane architectures and polymer–lipid interactions. Corresponding concentration profiles across the membranes obtained from the simulations are shown in Figure 3m–p.

The hydrophobic core thickness for neat lipid and polymer vesicles is measured as 3.4 and 10.6 nm, respectively (Figure 3e,h), in agreement with simulations (Figure 3m,p). At low (≤10 mol %) PBD-*b*-PEO type 2 phase separation is observed by thicker hydrophobic cores (7.2 nm) and higher electron density compared to pure lipid (Figure 3f,j,n), indicating that the lens-shape nanodomain contains PBD and lipid acyl chains. Furthermore, the lens domain is enclosed by electron-dense interfaces from continuous phospholipid monolayers.

At 20 mol % polymer, the hydrophobic core is thicker (8 nm) and the electron density is consistent with a polymer-rich domain in type 1 phase separation (Figure 3g,k,o). In both type 1 and type 2 phase separation, the direction of leaflet bending seen in electron density profiles and simulations (Figure S9) suggests some degree of leaflet compositional asymmetry[66] and potentially indicates that PEO chains are enriched in the outer leaflet.

From MD trajectories, the average membrane thickness (Figure 4a), the variance of the thickness (Figure 4b), order parameter (Figure 4c), and lipid area density (Figure 4d) were calculated across various lipid types and polymer concentrations (see Supporting Information for detailed descriptions of each calculation). The increase of average membrane thickness (Figure 4a) with polymer content is consistent with what is observed in the experiment. The linear increase can be attributed to the addition of a polymer in a collapsed state inside the lipid membrane. The deviation from a linear trend for DPPC:Chol:PBD-*b*-PEO points toward cholesterol partially mixing with the polymer-rich domains. The variance of the membrane thickness represents the surface roughness (Figure 4b), indicating the degree of domain formation. The simulation window for type 2 domain formation is ~5 mol % polymer for DPPC:Chol:PBD-*b*-PEO and between ~5 and 20 mol % polymer for both DPPC:PBD-*b*-PEO and DOPC:PBD-*b*-PEO (Figure 4e). Interestingly, all systems maintain similar order parameter (Figure 4c) in the region of type 2 domain stability, consistent with the ssNMR data.[10] The lipid area density (Figure 4d) displays similar trends. This implies that, in these simulations, the ordering of lipid tails is not significantly disrupted by unzipping around butadiene globules. Furthermore, type 2 morphologies are observed over a large range of lipid order and packing.

CONCLUSIONS

While the macroscopic phase separation of lipids and polymers inside coassembled hybrid membranes is well-characterized,[8,23,25,36–39] the understanding of molecular behavior and domain formation at the nanometer-length scale is still being developed.[52,54,55] Through the use of molecular-level characterization techniques, our findings support the hypothesis that for low polymer concentrations (5–10 mol %) and sufficiently large PBD blocks (around 45 monomers), bilayer unzipping (type 2 domains) is energetically more favorable than the hydrophobic mismatch that would be present in type 1 domains. Simulations show that this type 2 morphology is general, appearing in three unique lipid systems. Guided by the simulations, this work clearly demonstrates real-space images of nanometer-sized domains in hybrid vesicles.

These results and the presented methods directly contribute to the elucidation of nanoscale lateral phase separation processes and in-membrane interactions in hybrid membranes, which enable the design and programming of function in artificial membranes. More broadly, the discovery that lipid bilayers unzip to insert nanodomains of hydrophobic moieties offers new insights into the domain formation process in biological membranes. Given the similarities to biological processes, such as lipid droplets, we posit that the insertion of bulky hydrophobic transmembrane proteins might also induce type 2 phase separation. Domain and raft formation is a fundamental process in synthetic and biological

membranes that regulates selective transport, mechanical properties, and membrane binding recognition; this work greatly advances our understanding of it.

EXPERIMENTAL SECTION

Materials.

1,2-Dipalmitoyl-*sn-glycero*-3-phosphocholine (DPPC) and cholesterol (Chol), obtained from Avanti Polar Lipids (Alabama, USA), were dissolved in chloroform. The amphiphilic diblock copolymer, poly(butadiene-*b*-ethylene oxide) (PBD-*b*-PEO), with catalog number P19015-BdEO, was obtained from Polymer Source, Inc. (Quebec, Canada). The polydispersity index is 1.06, with an average molecular weight (Mn) of 4000 g/mol, comprising a PBD block (rich in 1,4 microstructure) weighing 2500 g/mol and a PEO block weighing 1500 g/mol, respectively. Our selection of PBD-*b*-PEO for this study was based on previous findings demonstrating the formation of phase-separated hybrid vesicles with distinct domains.[13,26,67]

Hybrid Nanoparticles (NPs) Formulation Using Microfluidic Device.

The self-assembly of NPs by microfluidics was accomplished by using the NanoAssemblr Benchtop platform (Precision Nanosystems Inc.). Ethanol solutions containing neat lipid (L) DPPC:Chol (10:5 wt/wt ratio equivalent to 50 mol %), pure block copolymer (BCP), and their hybrids at different L:BCP molar ratios (90:10 and 80:20 mol % of lipid to polymer) were dissolved at specific 8 mg/mL concentration. Through syringe pumps, the lipid/ethanol solution was introduced into one of the two channels on the microfluidics herringbone cartridge, while the aqueous phase was fed into the second channel. Microfluidics optimization involved adjusting the flow rate ratio (the ratio between the organic and aqueous phases) and the total flow rate (the speed at which the two channels were administered through the microfluidic chip) using NanoAssemblr software. A flow rate ratio of 1:2 and a total flow rate of 20 mL/min were selected to produce unilamellar vesicles. All production processes were conducted under ambient conditions, including room temperature and relative humidity.

The purification of samples was carried out using the Maxi 6000 Pur-A-Lyzer kit with a molecular weight cutoff (MWCO) of 6 kDa. To remove the solvent (EtOH), the samples were loaded into the Pur-A-Lyzer tube and then immersed in a stirred beaker filled with deionized (DI) water. The dialysis buffer was refreshed three times, with each change occurring every 3–4 h. All samples were recovered at their initial volume after purification.

Preparation of Cryogenic-Electron Microscopy (Cryo-EM) Grids and Subsequent Data Collection.

For cryo-EM, neat lipid, block copolymer, and hybrid samples were prepared on Cu Quantifoil grids (3.5/1, 200 mesh) from Electron Microscopy Sciences, using a Vitrobot Mark IV from Thermo Fisher Scientific. In brief, 4 μL of each sample was applied to the glow-discharged grid surface in a chamber maintained at 24 °C and 100% relative humidity followed by vitrification in liquid ethane. Prior to vitrification, samples were blotted for 6 s with a blot force of 1. Imaging of all cryo-EM grids was conducted using a 200 keV Glacios

TEM from Thermo Fisher Scientific, equipped with a Falcon4 direct electron detector. Images were captured at 73k× magnification (with a physical pixel size of 2.0 Å) and a defocus of −5 μm, utilizing Tomo automated acquisition software from Thermo Fisher.

Simulation Model and Methods.

We performed coarse-grained molecular dynamics simulations using HOOMD-blue[58] and parametrized with the Martini v3 force field.[57] Parametrization scheme is shown in Figure S1. This model has been used previously for PEO,[68–70] PBD,[55,71] cholesterol,[72] and phospholipids.[57] Validation of our implementations of the polymers is shown in Figure S2 and of the phospholipid:cholesterol membranes is shown in Figures S3 and S4. The simulated polymer PBD-*b*-PEO was represented with 46 PBD beads and 35 PEO beads.

Simulations were conducted in an *NPT* ensemble where the pressure in the *z* direction was maintained at 1 atm and the pressure in the *xy*-plane was held at 0 atm. The temperature was maintained at 298 K. A constant pressure barostat[73] and Nose–Hoover thermostat were used to maintain the pressure and temperature. A timestep of 20 fs was used, consistent with Martini simulations. Electrostatics were handled with the reaction field scheme with a cutoff distance of 1.1 nm simulations. Simulations were run for 10^7 timesteps or 0.2 μs.

Hybrid membranes were initialized randomly in a membrane-like morphology. Different initialization conditions are discussed in Figures S5 and S6 but form similar morphologies. All snapshots and 2D maps shown are representative of five uniquely randomized simulations. Likewise, the properties shown in Figure 4 were averaged from five unique simulations. Detailed discussion of analysis methods is given in Supporting Information section 1.2.

Supplementary Material

Refer to Web version on PubMed Central for supplementary material.

ACKNOWLEDGMENTS

This work was supported by the National Science Foundation under Grant CBET 2219305 and the National Institutes of Health under Grant R01GM143723 (lipid vesicle formulation) and National Institute of Diabetes and Digestive and Kidney Diseases under Grant R01-DK130317 (cryo-EM imaging of in-membrane hydrophobic domains). Cryo-EM imaging was conducted in the Materials Research Laboratory Central Research Facilities, University of Illinois at Urbana—Champaign (UIUC). We acknowledge Dr. Kristen Flatt for assistance with cryo-EM grids preparation and loading. J.F.T. and A.S. acknowledge funding received from the Grainger College of Engineering at UIUC. This work made use of the Illinois Campus Cluster, a computing resource that is operated by the Illinois Campus Cluster Program (ICCP) in conjunction with the National Center for Supercomputing Applications (NCSA) and which is supported by funds from UIUC.

REFERENCES

(1). Schwille P Bottom-up synthetic biology: engineering in a tinkerer’s world. Science 2011, 333, 1252–1254. [PubMed: 21885774]

(2). Gözen I; Köksal ES; Põldsalu I; Xue L; Spustova K; Pedrueza-Villalmanzo E; Ryskulov R; Meng F; Jesorka A Protocells: Milestones and recent advances. Small 2022, 18, 2106624.

(3). Tu Y; Peng F; Adawy A; Men Y; Abdelmohsen LK; Wilson DA Mimicking the cell: bio-inspired functions of supramolecular assemblies. Chem. Rev. 2016, 116, 2023–2078. [PubMed: 26583535]

(4). Vance JA; Devaraj NK Membrane mimetic chemistry in artificial cells. J. Am. Chem. Soc. 2021, 143, 8223–8231. [PubMed: 34014081]

(5). Discher BM; Won Y-Y; Ege DS; Lee JC; Bates FS; Discher DE; Hammer DA Polymersomes: tough vesicles made from diblock copolymers. Science 1999, 284, 1143–1146. [PubMed: 10325219]

(6). Israelachvili JN; Mitchell DJ; Ninham BW Theory of self-assembly of hydrocarbon amphiphiles into micelles and bilayers. Journal of the Chemical Society, Faraday Transactions 2: Molecular and Chemical Physics 1976, 72, 1525–1568.

(7). Bates CM; Bates FS 50th Anniversary Perspective: Block Polymers - Pure Potential. Macromolecules 2017, 50, 3–22.

(8). Schulz M; Glatte D; Meister A; Scholtysek P; Kerth A; Blume A; Bacia K; Binder WH Hybrid lipid/polymer giant unilamellar vesicles: effects of incorporated biocompatible PIB–PEO block copolymers on vesicle properties. Soft Matter 2011, 7, 8100–8110.

(9). Kang M; Lee B; Leal C Three-Dimensional Microphase Separation and Synergistic Permeability in Stacked Lipid–Polymer Hybrid Membranes. Chem. Mater. 2017, 29, 9120–9132. [PubMed: 31097879]

(10). Kang M; Tuteja M; Centrone A; Topgaard D; Leal C Nanostructured Lipid-Based Films for Substrate-Mediated Applications in Biotechnology. Adv. Funct. Mater. 2018, 28, 1704356.

(11). Tuteja M; Kang M; Leal C; Centrone A Nanoscale partitioning of paclitaxel in hybrid lipid–polymer membranes. Analyst 2018, 143, 3808–3813. [PubMed: 29878001]

(12). Go YK; Leal C Polymer–Lipid Hybrid Materials. Chem. Rev. 2021, 121, 13996–14030. [PubMed: 34752064]

(13). Kambar N; Leal C Microfluidic synthesis of multilayered lipid-polymer hybrid nanoparticles for the formulation of low solubility drugs. Soft Matter 2023, 19, 1596–1605. [PubMed: 36752169]

(14). Kang M; Go YK; Porras-Gomez M; Koulaxizis T; Steer D; Statt A; Leal C Cooperative Self-Assembly of Lipid–Polymer Hybrids Stabilizing Highly Ordered Bicontinuous Cubic Phases in Air. Macromolecules 2023, 56, 5774–5783.

(15). Kambar N; Go YK; Snyder C; Do MN; Leal C Structural characterization of lateral phase separation in polymer–lipid hybrid membranes. Methods Enzymol. 2024, 700, 235. [PubMed: 38971602]

(16). Brodszkij E; Städler B Advances in block copolymer-phospholipid hybrid vesicles: from physical–chemical properties to applications. Chem. Sci. 2024, 15, 10724–10744. [PubMed: 39027291]

(17). Jacobs ML; Boyd MA; Kamat NP Diblock copolymers enhance folding of a mechanosensitive membrane protein during cell-free expression. Proc. Natl. Acad. Sci. U. S. A. 2019, 116, 4031–4036. [PubMed: 30760590]

(18). Beales PA; Khan S; Muench SP; Jeuken LJ Durable vesicles for reconstitution of membrane proteins in biotechnology. Biochem. Soc. Trans. 2017, 45, 15–26. [PubMed: 28202656]

(19). Otrin N; Otrin L; Bednarz C; Träger TK; Hamdi F; Kastritis PL; Ivanov I; Sundmacher K Protein-Rich Rafts in Hybrid Polymer/Lipid Giant Unilamellar Vesicles. Biomacromolecules 2024, 25, 778–791. [PubMed: 38190609]

(20). Peruzzi JA; Steinkühler J; Vu TQ; Gunnels TF; Hu VT; Lu P; Baker D; Kamat NP Hydrophobic mismatch drives self-organization of designer proteins into synthetic membranes. Nat. Commun. 2024, 15, 3162. [PubMed: 38605024]

(21). Paxton WF; McAninch PT; Achyuthan KE; Shin SHR; Monteith HL Monitoring and modulating ion traffic in hybrid lipid/polymer vesicles. Colloids Surf., B 2017, 159, 268–276.

(22). Ozawa N; Kosaka S; Fujii S; Nishimura T Bilayer-domain formation of thermoresponsive amphiphilic block copolymers in hybrid liposomes for synthetic molecular channels. Polym. Chem. 2023, 14, 2198–2204.

(23). Go YK; Shin J; Chen G; Leal C Reorientation of Crystalline Block Copolymer Membranes by Phospholipid Hybridization. Chem. Mater. 2022, 34, 8577–8592.

(24). Monje-Galvan V; Voth GA Binding mechanism of the matrix domain of HIV-1 gag on lipid membranes. eLife 2020, 9, e58621. [PubMed: 32808928]

(25). Chemin M; Brun P-M; Lecommandoux S; Sandre O; Le Meins J-F Hybrid polymer/lipid vesicles: fine control of the lipid and polymer distribution in the binary membrane. Soft Matter 2012, 8, 2867–2874.

(26). Nam J; Beales PA; Vanderlick TK Giant Phospholipid/Block Copolymer Hybrid Vesicles: Mixing Behavior and Domain Formation. Langmuir 2011, 27, 1–6. [PubMed: 21133340]

(27). Nam J; Vanderlick TK; Beales PA Formation and dissolution of phospholipid domains with varying textures in hybrid lipo-polymersomes. Soft Matter 2012, 8, 7982–7988.

(28). Walther TC; Chung J; Farese RV Jr Lipid droplet biogenesis. Annual review of cell and developmental biology 2017, 33, 491–510.

(29). Li J; Zhang X; Cao D Decoupling of bilayer leaflets under gas supersaturation: nitrogen nanobubbles in a membrane and their implication in decompression sickness. J. Phys. D: Appl. Phys. 2018, 51, 184001.

(30). Bochicchio D; Panizon E; Monticelli L; Rossi G Interaction of hydrophobic polymers with model lipid bilayers. Sci. Rep. 2017, 7, 6357. [PubMed: 28744008]

(31). Von White GI; Chen Y; Roder-Hanna J; Bothun GD; Kitchens CL Structural and Thermal Analysis of Lipid Vesicles Encapsulating Hydrophobic Gold Nanoparticles. ACS Nano 2012, 6, 4678–4685. [PubMed: 22632177]

(32). Marzouq A; Morgenstein L; Huang-Zhu CA; Yudovich S; Atkins A; Grupi A; Van Lehn RC; Weiss S Long-Chain Lipids Facilitate Insertion of Large Nanoparticles into Membranes of Small Unilamellar Vesicles. Langmuir 2024, 40, 10477–10485. [PubMed: 38710504]

(33). Jung M; Hubert D; Bomans P; Frederik P; Meuldijk J; Van Herk A; Fischer H; German A New Vesicle–Polymer Hybrids: The Parachute Architecture. Langmuir 1997, 13, 6877–6880.

(34). Jung M; Hubert DHW; van Veldhoven E; Frederik P; van Herk AM; German AL Vesicle–Polymer Hybrid Architectures: A Full Account of the Parachute Architecture. Langmuir 2000, 16, 3165–3174.

(35). Hubert DHW; Jung M; German AL Vesicle Templating. Adv. Mater. 2000, 12, 1291–1294.

(36). Gettel DL; Sanborn J; Patel MA; de Hoog H-P; Liedberg B; Nallani M; Parikh AN Mixing, diffusion, and percolation in binary supported membranes containing mixtures of lipids and amphiphilic block copolymers. J. Am. Chem. Soc. 2014, 136, 10186–10189. [PubMed: 25003585]

(37). Dao TP; Brûlet A.; Fernandes F.; Er-Rafik M.; Ferji K.; Schweins R.; Chapel JP.; Fedorov A.; Schmutz M.; Prieto M.; Sandre O.; Le Meins JF. Mixing Block Copolymers with Phospholipids at the Nanoscale: From Hybrid Polymer/Lipid Wormlike Micelles to Vesicles Presenting Lipid Nanodomains. Langmuir 2017, 33, 1705–1715. [PubMed: 28128560]

(38). Go YK; Kambar N; Leal C Hybrid unilamellar vesicles of phospholipids and block copolymers with crystalline domains. Polymers 2020, 12, 1232. [PubMed: 32485809]

(39). Schulz M; Binder WH Mixed Hybrid Lipid/Polymer Vesicles as a Novel Membrane Platform. Macromol. Rapid Commun. 2015, 36, 2031–2041. [PubMed: 26457675]

(40). Di Leone S; Kyropoulou M; Köchlin J; Wehr R; Meier WP; Palivan CG Tailoring a Solvent-Assisted Method for Solid-Supported Hybrid Lipid–Polymer Membranes. Langmuir 2022, 38, 6561–6570. [PubMed: 35580858]

(41). Hamada N; Gakhar S; Longo ML Hybrid lipid/block copolymer vesicles display broad phase coexistence region. Biochimica et Biophysica Acta (BBA) - Biomembranes 2021, 1863, 183552. [PubMed: 33444620]

(42). Chen D; Santore MM Hybrid copolymer–phospholipid vesicles: phase separation resembling mixed phospholipid lamellae, but with mechanical stability and control. Soft Matter 2015, 11, 2617–2626. [PubMed: 25687473]

(43). Olubummo A; Schulz M; Schöps R; Kressler J; Binder WH Phase Changes in Mixed Lipid/Polymer Membranes by Multivalent Nanoparticle Recognition. Langmuir 2014, 30, 259–267. [PubMed: 24359326]

(44). Schulz M; Olubummo A; Bacia K; Binder WH Lateral surface engineering of hybrid lipid-BCP vesicles and selective nanoparticle embedding. Soft Matter 2014, 10, 831–839. [PubMed: 24837370]

(45). Cheng Z; Elias DR; Kamat NP; Johnston ED; Poloukhtine A; Popik V; Hammer DA; Tsourkas A Improved Tumor Targeting of Polymer-Based Nanovesicles Using Polymer–Lipid Blends. Bioconjugate Chem. 2011, 22, 2021–2029.

(46). Ruysschaert T; Sonnen AFP; Haefele T; Meier W; Winterhalter M; Fournier D Hybrid Nanocapsules: Interactions of ABA Block Copolymers with Liposomes. J. Am. Chem. Soc. 2005, 127, 6242–6247. [PubMed: 15853329]

(47). Schulz M; Werner S; Bacia K; Binder WH Controlling Molecular Recognition with Lipid/Polymer Domains in Vesicle Membranes. Angew. Chem., Int. Ed. 2013, 52, 1829–1833.

(48). Winzen S; Bernhardt M; Schaeffel D; Koch A; Kappl M; Koynov K; Landfester K; Kroeger A Submicron hybrid vesicles consisting of polymer–lipid and polymer–cholesterol blends. Soft Matter 2013, 9, 5883–5890.

(49). Brodszkij E; Westensee IN; Holleufer SF; Ade C; Andres PDD; Pedersen JS; Städler B Membrane composition of polymer-lipid hybrid vesicles. Applied Materials Today 2022, 29, 101549.

(50). Perera RM; Gupta S; Li T; Van Leeuwen CJ; Bleuel M; Hong K; Schneider GJ Nanoscale Lipid/Polymer Hybrid Vesicles: Effects of Triblock Copolymer Composition and Hydrophilic Weight Fraction. ACS Applied Polymer Materials 2022, 4, 8858–8868.

(51). Lim SK; De Hoog H-P; Parikh AN; Nallani M; Liedberg B Hybrid, nanoscale phospholipid/block copolymer vesicles. Polymers 2013, 5, 1102–1114.

(52). Seneviratne R; Coates G; Xu Z; Cornell CE; Thompson RF; Sadeghpour A; Maskell DP; Jeuken LJC; Rappolt M; Beales PA High Resolution Membrane Structures within Hybrid Lipid-Polymer Vesicles Revealed by Combining X-Ray Scattering and Electron Microscopy. Small 2023, 19, 2206267.

(53). Hu S-W; Huang C-Y; Tsao H-K; Sheng Y-J Hybrid membranes of lipids and diblock copolymers: From homogeneity to rafts to phase separation. Phys. Rev. E 2019, 99, 012403. [PubMed: 30780280]

(54). Müller WA; Beales PA; Muniz AR; Jeuken LJ Unraveling the Phase Behavior, Mechanical Stability, and Protein Reconstitution Properties of Polymer-Lipid Hybrid Vesicles. Biomacromolecules 2023, 24, 4156–4169. [PubMed: 37539954]

(55). Steinkühler J; Jacobs ML; Boyd MA; Villaseñor CG; Loverde SM; Kamat NP PEO- b-PBD Diblock Copolymers Induce Packing Defects in Lipid/Hybrid Membranes and Improve Insertion Rates of Natively Folded Peptides. Biomacromolecules 2022, 23, 4756–4765. [PubMed: 36318160]

(56). Olzmann JA; Carvalho P Dynamics and functions of lipid droplets. Nat. Rev. Mol. Cell Biol. 2019, 20, 137–155. [PubMed: 30523332]

(57). Souza PC; et al. Martini 3: a general purpose force field for coarse-grained molecular dynamics. Nat. Methods 2021, 18, 382–388. [PubMed: 33782607]

(58). Anderson JA; Glaser J; Glotzer SC HOOMD-blue: A Python package for high-performance molecular dynamics and hard particle Monte Carlo simulations. Comput. Mater. Sci. 2020, 173, 109363.

(59). Johnson BK; Prud'homme RK Chemical processing and micromixing in confined impinging jets. AIChE J. 2003, 49, 2264–2282.

(60). Johnson BK; Prud'homme RK Process and apparatuses for preparing nanoparticle compositions with amphiphilic copolymers and their use. U.S. Patent 8,137,699, 2012.

(61). Markwalter CE; Pagels RF; Wilson BK; Ristroph KD; Prud'homme RK Flash nanoprecipitation for the encapsulation of hydrophobic and hydrophilic compounds in polymeric nanoparticles. J. Visualized Exp. 2019, e58757.

(62). Kim H; Sung J; Chang Y; Alfeche A; Leal C Microfluidics synthesis of gene silencing cubosomes. ACS Nano 2018, 12, 9196–9205. [PubMed: 30081623]

(63). Heberle FA; Doktorova M; Scott HL; Skinkle AD; Waxham MN; Levental I Direct label-free imaging of nanodomains in biomimetic and biological membranes by cryogenic electron microscopy. Proc. Natl. Acad. Sci. U. S. A. 2020, 117, 19943–19952. [PubMed: 32759206]

(64). Cornell CE; Mileant A; Thakkar N; Lee KK; Keller SL Direct imaging of liquid domains in membranes by cryo-electron tomography. Proc. Natl. Acad. Sci. U. S. A. 2020, 117, 19713–19719. [PubMed: 32759217]

(65). Bello G; Cavallini F; Dailey LA; Ehmoser E-K Supported polymer/lipid hybrid bilayers formation resembles a lipid-like dynamic by reducing the molecular weight of the polymer. Biochimica et Biophysica Acta (BBA) - Biomembranes 2021, 1863, 183472. [PubMed: 32941874]

(66). Varma M; Deserno M Distribution of cholesterol in asymmetric membranes driven by composition and differential stress. Biophys. J. 2022, 121, 4001–4018. [PubMed: 35927954]

(67). Le Meins J-F; Schatz C; Lecommandoux S; Sandre O Hybrid polymer/lipid vesicles: state of the art and future perspectives. Mater. Today 2013, 16, 397–402.

(68). Grunewald F; Rossi G; de Vries AH; Marrink SJ; Monticelli L Transferable MARTINI Model of Poly(ethylene Oxide). J. Phys. Chem. B 2018, 122, 7436–7449. [PubMed: 29966087]

(69). Rossi G; Fuchs PF; Barnoud J; Monticelli L A coarse-grained MARTINI model of polyethylene glycol and of polyoxy-ethylene alkyl ether surfactants. J. Phys. Chem. B 2012, 116, 14353–14362. [PubMed: 23137188]

(70). Grünewald F; Alessandri R; Kroon PC; Monticelli L; Souza PC; Marrink SJ Polyply; a python suite for facilitating simulations of macromolecules and nanomaterials. Nat. Commun. 2022, 13, 68. [PubMed: 35013176]

(71). Alessandri R; Barnoud J; Gertsen AS; Patmanidis I; de Vries AH; Souza PC; Marrink SJ Martini 3 Coarse-Grained Force Field: Small Molecules. Adv. Theory Simul. 2022, 5, 2100391.

(72). Borges-Araújo L; Borges-Araújo AC; Ozturk TN; Ramirez-Echemendia DP; Fábián B; Carpenter TS; Thallmair S; Barnoud J; Ingólfsson HI; Hummer G; Tieleman DP; Marrink SJ; Souza PCT; Melo MN Martini 3 Coarse-Grained Force Field for Cholesterol. J. Chem. Theory Comput. 2023, 19, 7387–7404. [PubMed: 37796943]

(73). Martyna GJ; Tobias DJ; Klein ML Constant pressure molecular dynamics algorithms. J. Chem. Phys. 1994, 101, 4177–4189.

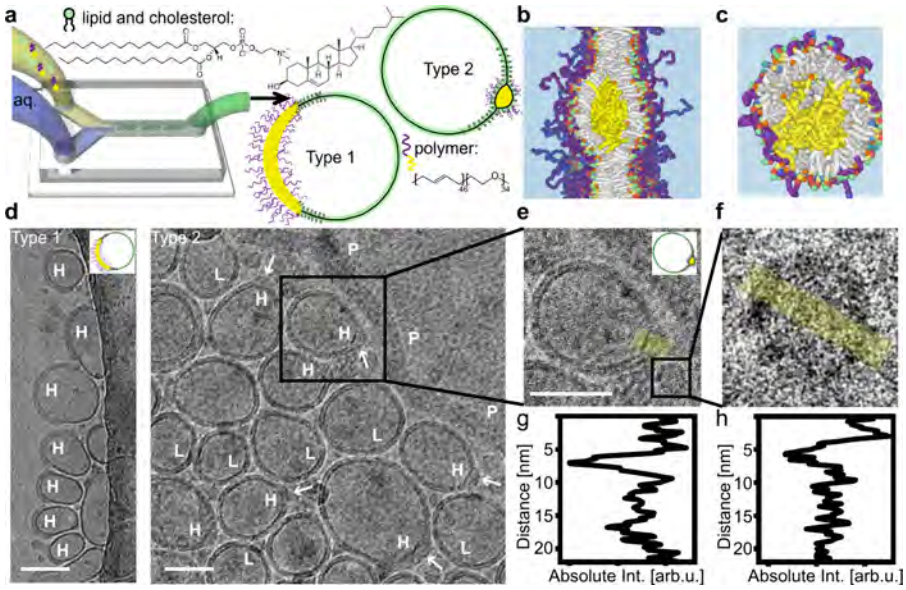

Figure 1.

Nanodomains in the hybrid membranes. (a) Schematics of microfluidic formulation of hybrid DPPC:Chol:PBD-*b*-PEO vesicles forming nanodomains. (b) MD snapshot of type 2 domain composed of DPPC:Chol:PBD-*b*-PEO (45:45:10 mol %). PBD (yellow), PEO (purple), lipid tails (gray), DPPC head (blue, pale yellow, red, green), cholesterol head (orange). (c) MD snapshot of a spherical hybrid micelle composed of DPPC:Chol:PBD-*b*-PEO (45:45:10 mol %). (d) Left: cryo-EM of type 1 hybrid (H) vesicles (DPPC:Chol:PBD-*b*-PEO, 40:40:20 mol %). Inset: Schematic representation of a type 1 hybrid vesicle. Right: cryo-EM images of three vesicle samples imaged on the same grid. Hybrid (H) DPPC:Chol:PBD-*b*-PEO (45:45:10 mol %), neat lipid (L) DPPC:Chol (50:50 mol %), and 100% PBD-*b*-PEO (P). White arrows indicate the localization of hybrid domains. (e) Enlarged view of a hybrid vesicle with a type 2 domain. Inset: Schematic representation of a type 2 hybrid vesicle. (f) Enlarged view of a hybrid micelle. (g) Absolute intensity profile showing the electron density across the vesicle membrane in (e). (h) Absolute intensity profile showing the electron density across the micelle in (f). Scale bars: 50 nm.

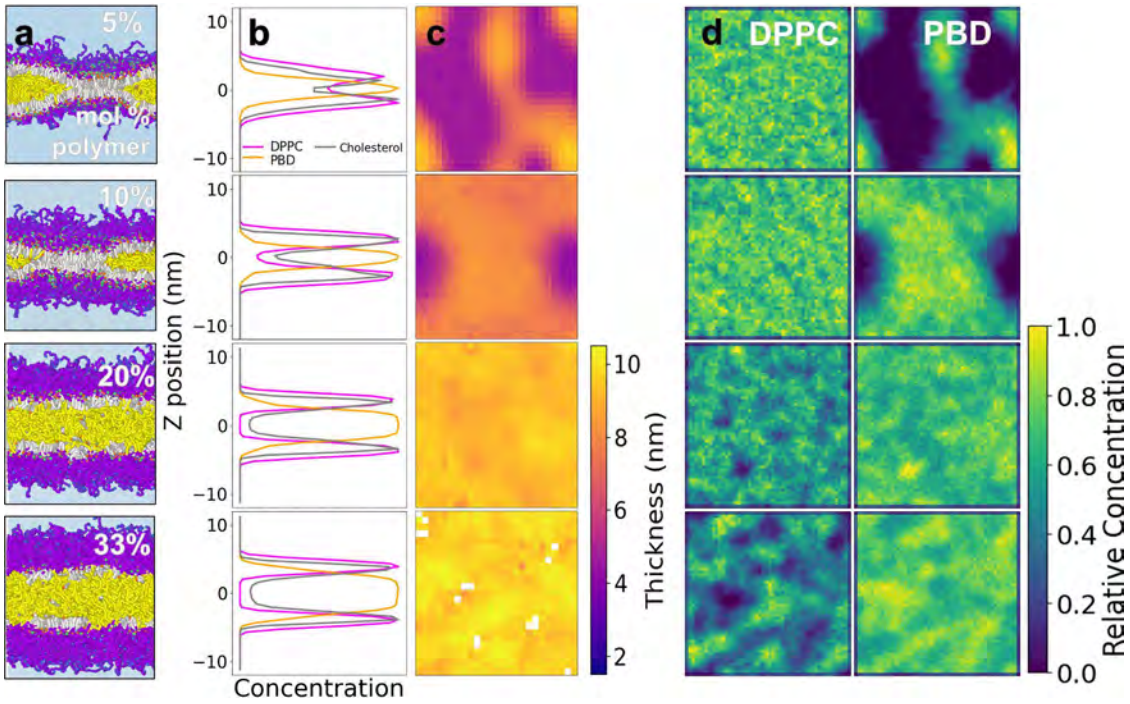

Figure 2.

Effect of increasing fraction of polymer (top to bottom) with respect to lipids in simulations. (a) Side snapshots of hybrid membranes. (b) Fraction of phospholipid, hydrophobic block of polymer, and cholesterol content across the membrane. (c) Phospholipid headgroup-to-headgroup thickness maps, where purple corresponds to thin and orange to thick regions and white pixels represent insufficient lipid concentration. (d) Concentration maps showing local concentration differences of two constituent materials (DPPC, PBD), where yellow is high and purple is low. Cholesterol follows the distribution of DPPC. PEO is dispersed relatively uniformly.

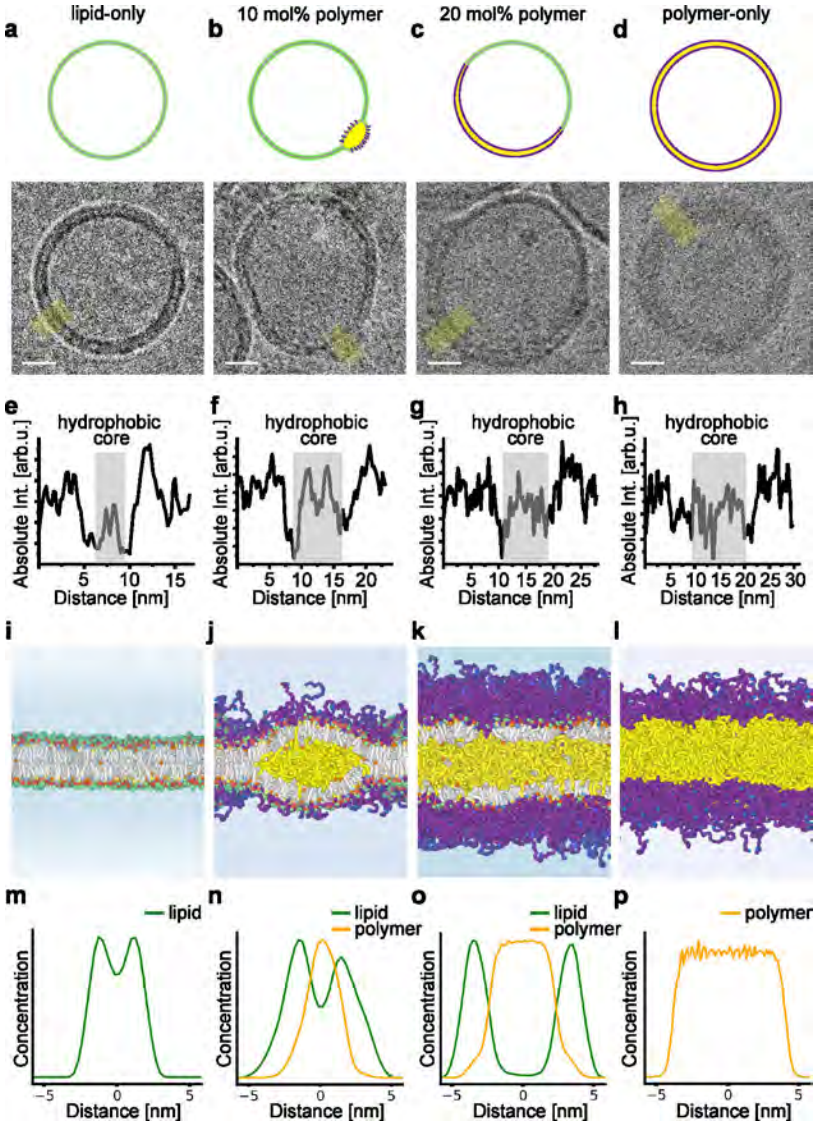

Figure 3.

Cryo-EM and simulation data obtained for hybrid membranes at different PBD-*b*-PEO contents. (a–d) Cryo-EM images of hybrid vesicles with increasing content of polymer (0, 10, 20, 100 mol % PBD-*b*-PEO). The inset cartoons at the top depict the domain morphology. (e–h) Averaged intensity profiles of the region highlighted by a semitransparent yellow box in (a)–(d) cryo-EM images, respectively. Gray boxes indicate the hydrophobic core of the bilayer. Scale bars: 10 nm. (i–l) Simulation snapshots of hybrid membranes with increasing polymer content (0, 5, 20, 100 mol % PBD-*b*-PEO). (m–p) Concentration profiles across the membrane. Green line shows lipid/cholesterol content, and yellow line shows PBD.

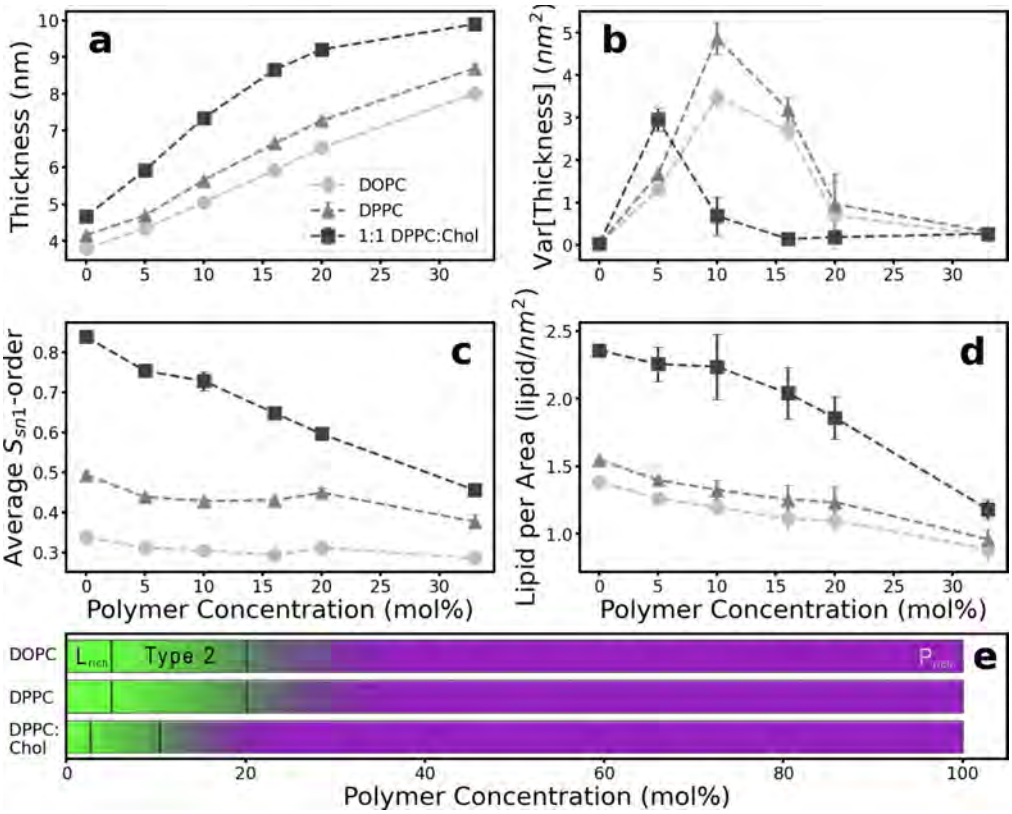

Figure 4.

Quantification of membrane properties across 3 lipid types as a function of polymer concentration. (a) Average membrane thickness, (b) variance of membrane thickness, (c) order parameter of sn1 phospholipid tails with respect to membrane normal, and (d) lipids per membrane surface area. (e) Diagram representing simulated morphology as a function of polymer concentration. Legend refers to panels a–d.